Int. J. Electrochem. Sci., 4 **(2009)** 1178 - 1195

International Journal of ELECTROCHEMICAL SCIENCE
www.electrochemsci.org

Critical Carbonation Depth for Initiation of Steel corrosion in Fully Carbonated Concrete and Development of Electrochemical Carbonation Induced Corrosion Model

Raja Rizwan Hussain [1*] *and Tetsuya Ishida* [2]

[1] Center of Excellence for Concrete Research and Testing, Civil Engineering Department, King Saud University, P.O.Box 800, 11421 Riyadh, Saudi Arabia
[2] Department of Civil Engineering, University of Tokyo, Japan
[*]E-mail: raja386@hotmail.com

Received: 30 June 2009 / *Accepted:* 11 August 2009 / *Published:* 25 August 2009

It is well known that carbonation of concrete initiates corrosion of reinforcing steel by lowering the pH value, but the extent and variety of possible damage has limited research data and there exists a difference of opinion between various researchers while defining the critical carbonation depth in relation to the initiation of steel corrosion in fully carbonated concrete. Therefore, in this research experiments were conducted under severe environments for carbonation progress and measurements were obtained for carbonation depth, corrosion potential and corrosion mass loss due to carbonation under air dry condition. Also, carbonation induced electrochemical corrosion model was developed by our research group at the University of Tokyo and its authenticity was checked in the light of experiment results obtained in this research. Combined with the measurement of carbonation depth, half-cell potential values were determined so that a relation can be developed between the carbonation depth and corrosion potential. The objective is to observe the behaviour of carbonation depth-corrosion potential profile and determine the critical carbonation depth if any. It is found that the corrosion potential values vary with time domain and depth of carbonation. The carbonation induced corrosion does not start until carbonation depth reaches a certain critical level from the steel rebar. Another interesting fact that was seen from the experiment results of this research is that the half-cell potential values after the carbonation reaches the rebar level rise again. The reason is sought to lie in the varying resistivity of carbonated concrete. Compared to chloride induced corrosion in general, the carbonation induced corrosion can be pronounced as a low rate of corrosion reaction. However, it should be mentioned here that in case of carbonation induced corrosion high relative humidity plays a decisive role. The comparison of carbonation induced electrochemical corrosion model analysis and experiment results shows a fair agreement. The carbonation induced electrochemical corrosion model reasonably predicts the behaviour of corrosion for normal air dry relative humidity conditions. The electrochemical model developed also shows fair qualitative simulation for various pH levels.

Keywords: critical carbonation depth, corrosion rate, half-cell potential, reinforced concrete, experimentation and modeling

1. INTRODUCTION

The carbonation induced corrosion of reinforced concrete is typically defined as the chemical reaction between atmospheric carbon dioxide, of which normal indoor concentration is approximately 370 ppmv and outdoor of 700 ppmv, and the product of hydration, mainly calcium hydroxide reducing the pH of concrete and destroying the passive layer on steel rebars which gives start to corrosion. Many researchers have investigated the phenomenon of carbonation and its effect on corrosion of reinforced concrete structures [1-6], but the extent of possible damage (maximum possible corrosion rate due to carbonation and critical carbonation depth) has limited research data. In this research qualitative as well as quantitative deep investigation has been carried out in order to clarify the mechanism of corrosion due to carbonation by experimentation and modeling approach.

2. MODELING

2.1. Mass Conservation Law for Carbon dioxide

Initially, the model is adopted from the previous research [7-10]. In general, when dealing with mass, energy and momentum flows in a control volume, the starting point is to build appropriate balance equations. In other words, the summation of rate of mass efflux from a control volume, the rate of mass flow into the control volume, and the rate of accumulation of mass within the control volume should be zero. In this section, the mass balance conditions for carbon dioxide in a porous medium are formulated. Two phases of carbon dioxide existing in concrete are considered; gaseous carbon dioxide and carbon dioxide dissolved in pore water. By solving the mass balance equation under given initial and boundary conditions, the non-steady state conduction of carbon dioxide is quantified. The mass balance equation for a porous medium can be expressed as Eq. 1.

$$\partial/\partial t\{\emptyset[1-S)\cdot\rho_{\mathbf{1}}g+S\cdot\rho_{\mathbf{1}}d]\}+dtvJ_{\mathbf{1}}(\ [\![CO]\!]_{\mathbf{1}}2\ )-Q_{\mathbf{1}}(\ [\![CO]\!]_{\mathbf{1}}2\ )=0 \quad (1)$$

Where,

$\emptyset$ is porosity of the porous media

S is degree of saturation of the porous media

ρ_d is density of dissolved CO_2 in pore water (kg/m^3)

ρ_g is density of gaseous CO_2 (kg/m^3)

J_{co_2} is total flux of disolved and gaseous CO_2 (kg/m^2s)

Q_{co_2} is the sink term which represents the rate of CO_2 consumption due to corrosion (kg/m^3s)

The above equation gives the concentrations of gaseous and dissolved carbon dioxide with time and space.

2.2. Equilibrium Conditions for Gaseous and Dissolved Carbon Dioxide

The local equilibrium between gaseous and dissolved carbon dioxide is represented here by Henry's law, which states the relationship between gas solubility in pore water and the partial gas pressure. In this research, it is assumed that the system will instantaneously reach local equilibrium between the two phases as Eq. 2. [11].

$$P_{CO_2} = H'_{CO_2} \cdot \rho'_d \tag{2}$$

Where,

P_{CO_2} is equilibrium partial pressure oxygen in the gas phase

ρ′d is mole fraction of gaseous CO_2 [mol of CO_2/total mol of solution]

H'_{CO_2} is Henry's constant for carbon dioxide (=4.06×109 [Pa/mol fraction] at 25℃)

For one cubic meter of dilute solution, the moles of water in the solution n_{H_2O} will be approximately 5.56×104[mol/m^3]; accordingly the concentration of dissolved carbon dioxide per cubic meter of solution ρ_d [kg/m^3] can be expressed as Eq. 3.

$$\rho_d = \frac{P_{CO_2}}{H'_{CO_2}} \cdot n_{H_2O\,0} \cdot M_{CO_2} = \frac{P_{CO_2}}{H_{CO_2}} \tag{3}$$

Where, M_{CO_2} is the molecular mass of carbon dioxide (= 0.044[kg/mol]).

The complete perfect-gas equation is then,

$$P_{CO_2} = \rho_g \frac{RT}{M_{CO_2}} \tag{4}$$

Where, ρg: concentration of gaseous oxygen [kg/m^3], R: gas constant [J/mol.K], and T: temperature [K]. From above Eqns. the equilibrium relationship between gas and dissolved CO_2 can be expressed as,

$$\rho_g = \frac{M_{CO_2}}{RT} \cdot H_{CO_2} \cdot \rho_d = K_{CO_2} \cdot \rho_d \tag{5}$$

After dissolving into solution, carbon dioxide reacts with calcium ions, and so the concentration of dissolved CO_2 can fluctuate from the above equilibrium condition. Strictly speaking, therefore, the equilibrium condition cannot be formulated by Henry's law alone; it is also necessary to determine the amount of dissolved CO_2 based on the rate of chemical reactions, which represents kinetic fluctuations dependent on the distribution of CO_2 concentration. However, it seems difficult to take into account

such kinetic fluctuations as it is, and in fact, it is expected that the rate of CO_2 gas dissolution will be faster when the partial pressure of CO_2 gas becomes large. For these reasons, in the model it is assumed that the amount of dissolved CO_2 can be approximately described by Henry's law [12],[13].

2.3. Carbon Dioxide Transport

Transport of CO_2 is considered for both dissolved and gaseous carbon dioxide phases. The CO_2 gas can move through unsaturated pores, whereas dissolved CO_2 is transported within pore liquid water. In the model, it is assumed that all pores have a cylindrical shape. Diffusion in a porous body may occur by one or more of three mechanisms: molecular diffusion (Fick diffusion), Knudsen diffusion, and surface diffusion. In the model, molecular diffusion and Knudsen diffusion are considered, whereas the contribution of surface diffusion is ignored, since surface diffusion takes places when molecules which have been adsorbed are transported along the pore wall, and normally it plays a minor role in diffusion within concrete materials under typical environmental conditions [14],[15],[16]. As the relative humidity in a pore decreases, the porous medium for gas transport becomes finer. If the pores through which the gas is traveling are quite small, the molecules will collide with the walls more frequently than with each other. This is known as Knudsen diffusion. The conditions transiting to Knudsen diffusion are expressed by the following equation using Knudsen number N_k as,

$$N_k = \frac{l_m}{2r_e} > 1.0 \tag{6}$$

Where, l_m: the mean free path length of a molecule of gas, and r_e: the actual pore radius, which means the radius of a pore minus the thickness of the adsorbed layer of water obtained by B.E.T. theory [11]. Considering molecular diffusion and Knudsen diffusion, the one dimensional gaseous flux through a single pore of radius *r* can be expressed as,

$$J_g^r = -\frac{D_o^g}{1 + \left(\frac{l_m}{2r_e}\right)} > \frac{\partial \rho_g}{\partial_x} \tag{7}$$

Where, D_0^g [m^2/s] is the diffusivity of CO_2 in a free atmosphere (=1.34×10^{-5}) [11]. Similarly, the flux of dissolved carbon dioxide can be obtained as

$$J_d^r = -D_0^d \frac{\partial \rho_d}{\partial_x} \tag{8}$$

Where, D_0^d [m^2/s] is the diffusivity of dissolved CO_2 in pore water (=1.0×10^{-9}) [11].

The total flux within porous bodies can be obtained by integrating the above equations over the entire porosity distribution. For example, consider the equilibrium condition of moisture during a monotonic wetting phase, in which there is no inkbottle effect [8]. In this case, based on the thermodynamic conditions, a certain group of pores whose radii is smaller than the specific radius r_c at which a liquid-vapor interface forms are completely filled with water, whereas larger pores remain empty or partially saturated so that these pores can be routes for the transfer of CO_2 gas. Therefore, by integrating the gaseous and dissolved fluxes of CO_2, respectively, the entire flux of carbon dioxide is formulated as,

$$J_{CO_2} = -\left[(\phi D_d O^T d)/\Omega \int_0^{r_c} \left(dV\,(\partial \rho_d)/\partial x\right) + (\phi D_g O^T g)/\Omega \int_0^{r_c} \omega\, dV/(1 + N_k)\right] \quad (9)$$

Where, V is the pore volume, and $\Omega = (\pi/2)^2$ accounts for the average tortuosity of a single pore as a fictitious pipe for mass transfer. The latter parameter considers the tortuosity of a hardened cement paste matrix, which is uniformly and randomly connected in a 3-D system [14]. The first term of the right-hand side in the above equation denotes the diffusive component of dissolved carbon dioxide in the pore liquid, whereas the second term represents the component of gaseous diffusion. The substitution of porosity saturation S for the integrals in the above equation in order to generalize the expression for an arbitrary moisture history gives,

$$J_{co_2} = -\left(D_{dco_2} \nabla P_d + D_{gco_2} \nabla P_g\right) = -\left(D_{gco_2} K_{co_2} + D_{dco_2}\right) \nabla P_d \quad (10)$$

$$D_{gco_2} = \frac{\phi D_0^g}{\Omega} \frac{(1 - S)}{1 + \frac{l_m}{2(r_m - r_t)}} \quad , D_{dco_2} = \frac{\phi S D_0^d}{\Omega}$$

Where,

D_{gco_2} is diffusion coefficient of gaseous CO_2 in a porous medium [m^2/s]

D_{dco_2} is diffusion coefficient of dissolved CO_2 in a porous medium [m^2/s]

In the above equation, integral of the Knudsen number is simplified so that it can be easily put into practical computational use; r_m is the average radius of unsaturated pores, and t_m is the thickness of the adsorbed water layer in the pore whose radius is r_m. It has to be noted that the above formulations do not include the complete effects of the connectivity of pores on diffusivity. That is to say, considering one-dimensional transport of gaseous phases, all unsaturated pores, which are route for gas movement, are assumed to be connected with perfect continuity (Fig.1, left) [7]. In actual pore structures that have complicated connectivity, however, the movement of gas will be blocked by saturated pores containing liquid water (Fig.1, right). Here, as the saturation of pores decreases, the open pore space gains higher connectivity so that total diffusivity increases nonlinearly. One potential model for this phenomenon would be based on percolation theory [17]; however, we adopt the following model for the sake of

simplicity. In the future, research is needed to be done especially on this section of the model in order to make it more close to the reality by including the actual complexity of the concrete pores and its interconnectivity as well as discontinuity. Yet, is worth mentioning here that the simplified theory adopted in this research is based on the actual complex constrictivity and tortuosity of the concrete micro-structure.

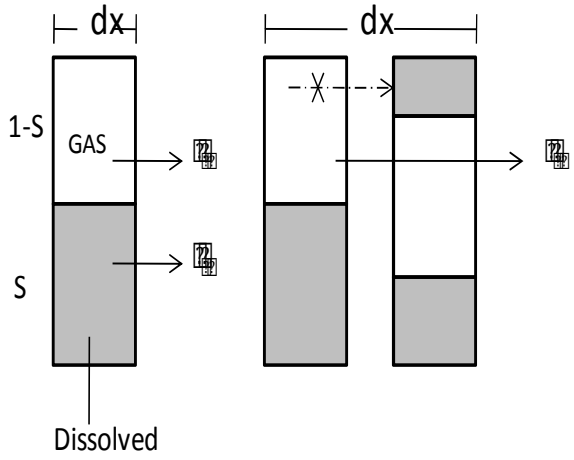

Figure 1. Effect of Connectivity of pores on CO_2 transport

Consider a finite field that consists of segments small enough to have continuity of pores, as shown in Fig.1, right. In the cross section of each unit, the ratio of gas transportation paths will be (1-S). If we assume that the probability of unsaturated pores being connected to each other would be proportional to the ratio of the volume in a cross section, the overall flux can be expressed as,

$$D_{dco_2} = \frac{\emptyset D_O^g}{\Omega} \frac{(1-S)}{1+\frac{l_m}{2(r_m - r_t)}}. \qquad D_{dco_2} = \frac{\emptyset S D_O^d}{\Omega}$$

(11)

2.4 Enhanced electro-chemical model for simulation of carbonation induced corrosion rate

In this paper the model is enhanced from the previous research [7-10] by adding the calculation module for carbonation induced corrosion rate and potential modeling by taking into account the variation in pH value of concrete caused by carbonation reaction as a function of corrosion potential and corrosion current. Nernst equation describes the potential of electrochemical cell as a function of

concentrations of ions taking part in the reaction. The electro-chemical model enhancement based on Tafel's Law is discussed in the following sections:

2.4.1. Power of hydrogen ion concentration

The pH of a solution is a measure of the molar concentration of hydrogen ions in the solution and as such is a measure of the acidity or basicity of the solution. The letters pH stand for "power of hydrogen" and the numerical value is defined as the negative base 10 logarithm of the molar concentration of hydrogen ions.

$$pH = -\log_{10}[H^+] \tag{12}$$

2.4.2. Corrosion potential model

The measurement of the pH of a sample can be done by obtaining the cell potential of that sample in reference to a standard hydrogen electrode, as in the accepted procedure for measuring standard electrode potentials. This procedure would give a value of zero for a 1 Molar solution of H^+ ions, so that defines the zero of the pH scale. The cell potential for any other value of H^+ concentration can be obtained with the use of the Nernst equation. For a solution at 25°C this gives

$$E_{cell} = -0.0592 \log_{10}[H^+] \tag{13}$$

For this expression, a base change from the natural log to the base 10 logarithm was made in the Nernst equation. For constant temperature expression 'RT/F' has a constant value. In most cases, the activity of hydrogen ions in solution can be approximated by the Molar concentration of hydrogen ions ($[H^+]$) in a solution. To simplify calculations it is often combined with conversion factor between natural logarithm (denoted here by ln) and decimal logarithm (denoted here by log) to form value of '0.0591' (for 25°C). Here in this model the value has been rounded off to '0.06' for simplicity. To be precise one should not use concentrations, but thermodynamic activities of the ions present in the solution. When applied to the full cell formed from half cells present on inside and outside of glass [18], [19], Nernst equation takes form as shown in Equation 14. It is a known fact that any cell potential is a function of concentration of species. Therefore when the concentration of hydrogen ion varies which is actually the variation of pH, the cell potential also varies accordingly as shown by Equation 14 below.

$$E_{02}=E_{02}^{\Theta}+((RT/z_{02}F)\ln(P_{02}/P^{\Theta})-0.06pH \tag{14}$$

Where; pH: power of hydrogen ion concentration (12.3 for non-carbonated concrete in the model), E_{O2}: standard cell potential of O_2, cath. (V,SHE) , E_{O2}^{Θ}: standard cell potential of O_2 at 25°C (=0.40V), z_{O2}: the number of charge of O_2 (=2), P^{Θ}: atmospheric pressure, T: surrounding temperature in Kelvin scale.

2.4.3. Pourbaix diagram

In general, the relation between potential and pH value is given by pourbaix diagram. Based on thermodynamic conditions, the state of passive layer is evaluated by the pourbaix diagram, where steel corrodes, areas where protective oxides form, an area of immunity to corrosion depending on pH and the potential of steel reinforcement (Fig.2). Usually, the Pourbaix diagrams can be used for different types of functions. One is the predominance area diagram, in which the dominant aqueous species will be given as a function of pH and E, where pH means –log $a(H^+)$ and E is the corresponding variable for electrical potential. Resulting area of each aqueous species can be expressed in terms of convex polygons.

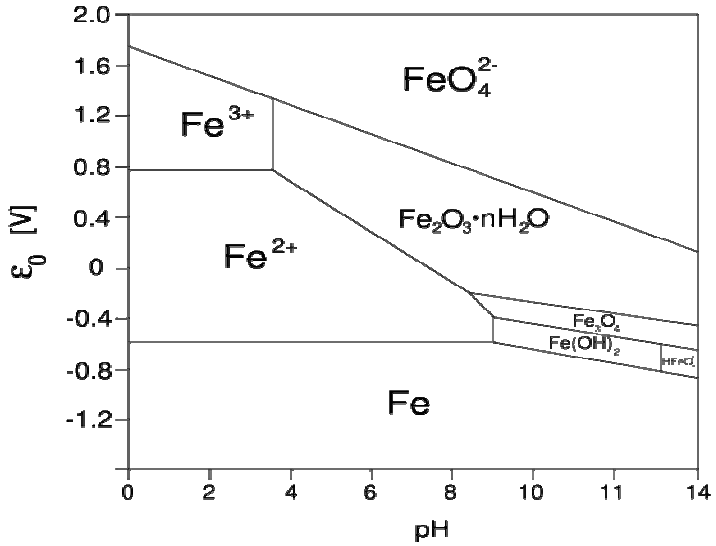

Figure 2. Pourbaix diagram relation between pH and potential state

2.4.4. Thermodynamics

In the present corrosion model, through the use of thermodynamic theory (the Nernst equation), so-called Pourbaix diagrams are constructed. These diagrams show the thermodynamic stability of species as a function of potential and pH. Although many basic assumptions must be considered in

their derivation, such diagrams can provide valuable information in the modeling of carbonation induced corrosion phenomena.

2.4.5. Corrosion Rate Model

As shown in Fig. 3 a decreasing trend of pH shifts the cathodic line diagonally towards the upward-rightward position. Thus, moving the point of intersection between cathode and anode lines towards the more corrosion current side. This answers the electro-chemical reason for the increase in corrosion rate due to decrease in pH caused by carbonation of concrete surrounding the rebar.

2.4.6. Limitations of Carbonation Induced Corrosion Model

Limited information on corrosion kinetics is provided by this model. The model is derived for specific temperature and pressure conditions. The model works for selected concentrations of ionic species. The model considers pure substances only and additional computations must be made if other species are involved. In areas where the model shows oxides to be thermodynamically stable, these oxides are not necessarily of a protective (passivating) nature.

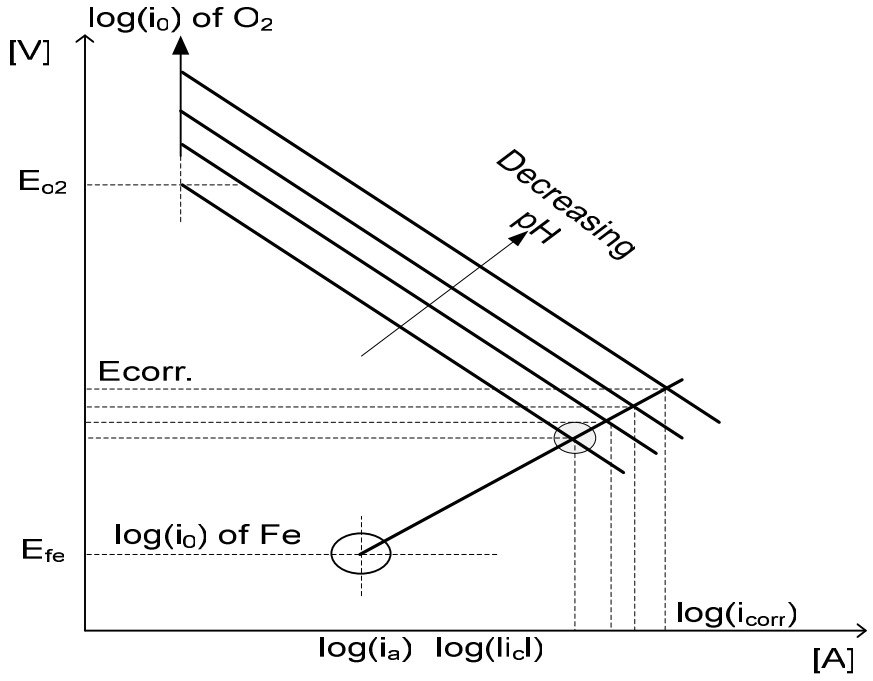

Figure 3. Modeling of carbonation induced corrosion (relation b/w pH and oxidation cell potential).

3. NUMERICAL SIMULATION

The above numerical formulations were analyzed for typical cases having the following data.

3.1. Basic Concrete Data for Model Analysis

The concrete composition was considered to consist of 371 kg/m^3 of OPC (Ordinary Portland Cement) as per JIS R5210 specifications with Water/Cement ratio (W/C) = 0.45. The chloride content was varied from 0%-8% free chloride by mass of binder in the analysis. The aggregates were considered as natural river sand passed through JIS A1102 sieve No. 4 (4.75-mm openings) used as fine aggregate for all concrete mixes numerical analysis data input. Its density and water absorption were considered to be 2.65 g/cm^3 and 2.21%, respectively. Crushed limestone with a maximum size of 20 mm was considered as coarse aggregate with density of 2.70 g/cm^3 and water absorption 0.59%.

3.2. Modeling of Environmental Exposure Conditions

Most severe environmental conditions for maximum carbonation rate were modelled consisting of accelerated 10% carbon dioxide concentration in the environment, 30^{0}C temperature and 55% Relative humidity (R.H).

3.3. Simulation Results

The model is analyzed using the above mentioned data and simulation results are obtained for various pH values ranging from 14-7.0 as shown in Fig. 4. It can be seen that the model reasonably predicts the behaviour of carbonation induced corrosion qualitatively. The corrosion rate of un-carbonated concrete (assumed at pH 12.3) is lowest and the corrosion rate increases gradually with the fall in pH reaching the maximum corrosion rate at pH 7.0 where the pore solution becomes acidic and highly susceptible to corrosion in nature. In general, the pH value of carbonated concrete is less than 9. Therefore, it can be said that the corrosion rates represented by the curves of pH 9.0 or less are under coupled attack of chloride and carbonation corrosion.

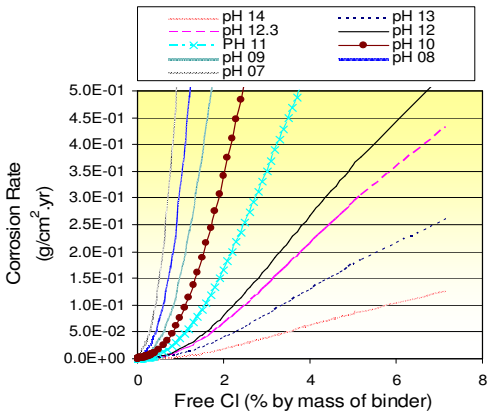

Figure 4(a) Coupled Cl and CO_2 (Small scale)

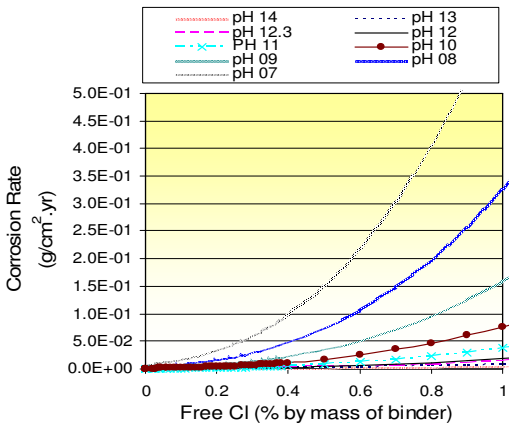

Figure 4(b) Enlarged scale

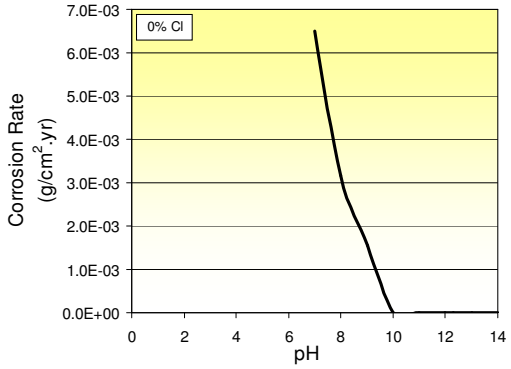

Figure 4(c) 0% Cl concentration

Figure 4. Analytical results of Carbonation induced corrosion model

3.4 Need for Experimental Verification

One more aspect which can be seen from these simulations is that under the coupled effect of chloride and carbonation, the corrosion rate is very high. But, when the chloride concentration is zero or very low, the carbonation induced corrosion rate is very low. In order to check in reality if this fact is true that the corrosion rate due to carbonation only is very low and to investigate some other related factors mentioned in the next section, following experiments were conducted.

4. EXPERIMENTATION

4.1. Objective

The objectives of this experimentation are:

a) Determination of extent of maximum corrosion rate in fully carbonated reinforced concrete

b) Determination of the relation between half-cell potential and carbonation depth

c) Determination of the critical carbonation depth

d) Verification of carbonation induced corrosion model

4.2. Mix Proportions

Trial concrete mixing is firstly conducted as per JCI mix design to achieve 05-08 cm of slump value and 3.5±1 % of air content. The concrete is composed of 371 kg/m^3 of OPC with Water/Cement ratio of 0.45. Coarse aggregate was 1031 kg/m^3 and fine aggregate proportion was 756 kg/m^3 of concrete.

4.3. Experiment Scheme

RC specimens were carbonated in carbonation chamber controlled at 10% of carbon dioxide concentration, 30 degree Centigrade temperature and 55% R.H. Please note that actual concentrations of carbon dioxide are approximately 0.03% in an outdoor atmosphere and 0.07% in an indoor atmosphere. The specimens were cured for 28 days under sealed conditions and 20 ℃ temperature before transferring to the carbonation chamber. Concrete specimens were cast with and without reinforcement steel. The specimens with reinforcement steel were used to measure half-cell potential and corrosion rate while the specimens without steel were used to measure carbonation depth by cutting slice of concrete specimen and spraying phenolphthalein indicator every time the measurement was taken.

In this experiment prismatic specimens of 200x100x100mm (L x W x H) size were made. Thin concrete cover of 13 mm was used to enable faster carbonation access from the surface of concrete to the rebar. The specimens were sealed and cured for 28 days at 20^0C temperature. Schematic diagram of the prismatic concrete specimen with and without steel bars is shown in the Fig. 5. The reinforced specimen has two 13mm diameter steel bars, one emerging out from two side for half-cell potential measurement and the other completely submerged into the concrete for gravimetric mass loss determination.

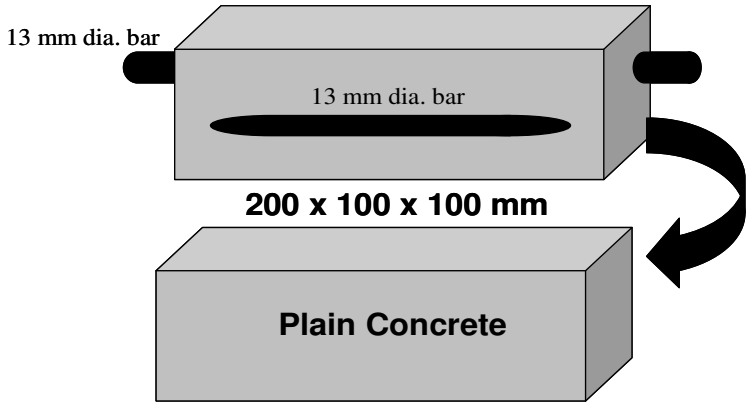

Figure 5. Test specimens shown with and without rebars

The reason for using two steel bars was to make it possible to measure corrosion potential and corrosion mass loss using the same specimen accurately. The bar emerging out from the two sides can be used for the corrosion potential measurement only since the two edges are not embedded into the concrete and are not under chloride attack. Therefore, in order to find the mass loss using the same specimen a separate steel bar was embedded completely into the concrete. This was done to obtain more reliable and accurate results. Concrete was poured in four layers alternated by tamping before pouring the second layer and so on until the fourth layer. Prior to coating bulging out ends of rebars by epoxy, steel reinforcement was connected to electric wires with the help of solder for measuring half-cell potential. Since carbonation is a slow process, therefore, in this experimentation the specimens are

carbonated by keeping them in a carbonation chamber set at accelerated carbonation conditions of 10% CO_2 concentration. Therefore, it should be noted that any conclusion drawn relate only to the experiment as described.

5. EXPERIMENT OBSERVATIONS

Carbonation depth and half-cell potentials were measured at specified time intervals. The carbonation depth was measured by cutting a thin slice of concrete specimen without rebar and then phenolphthalein indicator was sprayed over the freshly cut surface to measure the carbonation depth. Half-cell potential was measured using a copper-copper sulfate reference electrode (CSE), in accordance with ASTM C-876[20]. Finally the specimens were broken and corrosion mass loss was determined by gravimetric method after chemical cleaning of the corrosion products.

5.1. Carbonation Depth Measurement

In order to measure depth of carbonation, plain concrete specimens were periodically cut by the concrete cutting machine consecutively with the potential measurement so that a graph can be drawn for the relation between carbonation depth and half-cell potential. After cutting a fresh slice of concrete phenolphthalein in alcohol solution, which is colourless in acidic solution and changed to purple colour after pH decreased below 9, was sprayed to the freshly cut surface of concrete, noncarbonated areas turn to purple colour while carbonated areas remain colourless. Carbonation depths were averaged from 4 different measured points along the cut surface.

5.2. Half-Cell Potential Measurements for Carbonation Induced Corrosion

The copper-copper sulfate half-cell corrosions survey technique as outlined in ASTM C- 876-91 [20], is commonly used to investigate deteriorating structures, particularly structures that show signs of corrosion of uncoated reinforcing bars. The measurement of half-cell potential acts as a gauge of the corrosion being developed in R.C structures. An electrical connection is first made to the reinforcing steel. The potential difference on the concrete surface and the underlying reinforcement is measured.

5.3. Carbonation Induced Corrosion Mass Loss Measurement

After complete carbonation and completion of required post-carbonation exposure duration, the specimens were split along the position of steel in concrete and steel bars completely embedded in concrete for gravimetric mass loss calculation were removed. Following the photographic documentation of bar condition, the specimens were subjected to aggressive cleaning in accordance

with ASTM G1-03, method C.3.1 [21] and weighed to the nearest 0.0001 gram immediately after drying using standard systematic step by step cleaning method. The following Fig. is an illustration of experiment and observation.

6. EXPERIMENT RESULTS AND DISCUSSIONS

In this paper three experimental observations are given, namely carbonation depth, half-cell potential and gravimetric corrosion mass loss. All the three experimental observations were taken consecutively so that the carbonation induced corrosion reaction behaviour of steel in concrete can be observed in a three dimensional unified time and space domain. This is the originality of this experimentation. Each of the three experiment observations are discussed in detail in the following pages.

6.1. Carbonation Depth and Half-Cell Potential

Carbonation depth was measured by spraying phenolphthalein on freshly cut surface of specimen as shown in Fig. 6. Unchanged colour zone shows carbonated portion of concrete, while changed to purple portion shows non-carbonated zone. Because two surfaces were not coated by epoxy, carbonation depths were measured at four different points from both exposed surfaces. Their average values have been determined and presented in this paper. Combined with measurement of carbonation depth, half-cell potential values were also determined so that a relation can be developed between carbonation depth and half-cell potential. The idea was to observe the behaviour of carbonation depth-corrosion potential profile and determine the critical carbonation depth if any.

Figure 6. Experimental carbonation depth measurement

The results of experimental measurements for two prototype specimens (Specimen # 1 and 2) are shown in Fig. 7 below.

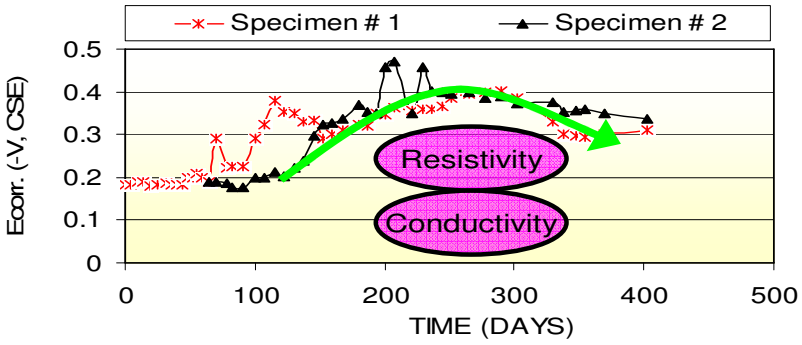

Fig. 7(a) Half-cell potential measurements as a function of time

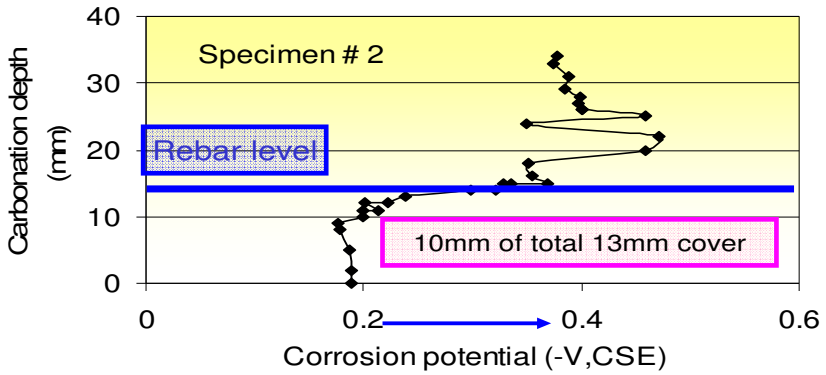

Fig. 7(b) Half-cell potential as a function of carbonation depth

Figure 7. Coupled carbonation induced corrosion experiment data

It can be seen from Fig. 7 that the half-cell potential values vary with time duration and depth of carbonation. The half-cell potential values are roughly above -200mV CSE until the carbonation reaches near steel bar which has 13 mm concrete cover. It can be seen that when carbonation reaches just before the level of rebar i.e. at 10 mm the half-cell potential suddenly falls from about -200mV to -400mV CSE until it reaches the surface of reinforcement bar. Before that the half-cell potential seems almost constant throughout the 10 mm concrete cover. It means that 10 mm is the critical carbonation depth at which the corrosion level rises suddenly. Therefore, it can be said that the carbonation induced corrosion does not start until the carbonation depth reaches a certain critical level of depth from the steel rebar. As rough approximation, it can be said that this critical carbonation depth is 80% (10mm/13mmx100=77%) of the total depth of concrete cover.

Another interesting fact that was seen from the experiment results shown in Fig. 7 is that the half-cell potential values after the carbonation reaches the rebar level rise again. It can be seen from the Fig. 7 that the half-cell potential after reaching the peak negative value of -475mV CSE raises again back to -320mV CSE. The reason is sought to lie in the varying resistivity of carbonated concrete. With the progress of carbonation reaction, resistivity of concrete increases which reduce the electrolytic conductivity of the pore solution resulting in reduction of corrosion rate. Therefore, it can be said that the carbonation induced corrosion has a falling trend with the passage of time.

6.2 Carbonation Induced Corrosion Mass Loss

Finally, the two identical specimens were broken and embedded steel bars were taken out for gravimetric corrosion mass loss determination. This mass loss was converted to corrosion rate by using Faraday's law. The results are shown in Fig. 8. The corrosion rate of the two specimens lies in general around 3.25×10^{-3} g/cm^2.yr which corresponds to 0.325μA/cm^2 of corrosion current. Compared to chloride induced corrosion in general this value is not very high and can be pronounced as a low rate

of corrosion. However, it should be mentioned over here that in case of carbonation induced corrosion high relative humidity (R.H) plays a decisive role. Due to the increased resistivity and reduced electrolytic conductivity of carbonated concrete, it needs high relative humidity to maintain high rates of corrosion. Since the specimen were exposed to 55% R.H during carbonation and 60% R.H after full carbonation until the end of experiment, the corrosion rates obtained by carbonation induced corrosion are in the low range. It is believed [22] that 80% R.H is ideal for producing high corrosion rates due to carbonation. Therefore, in the future research carbonation induced corrosion rate should be calculated experimentally for high relative humidity conditions more than 80% R.H.

7. VERIFICATION OF CARBONATION INDUCED CORROSION MODEL

The comparison of carbonation induced corrosion model analysis and experiment results shows fair agreement as shown in Fig. 8. It should be noted over here that carbonation induced corrosion starts at pH levels below 9.0. Since the pH level of the concrete was not measured in the experiment, therefore, in the comparison it is tentatively assumed that the pH of carbonated concrete is 8.0. It can also be seen (Fig. 4) that the model reasonably predicts the behaviour of carbonation induced corrosion at various pH levels and coupled chloride-carbonation effects qualitatively.

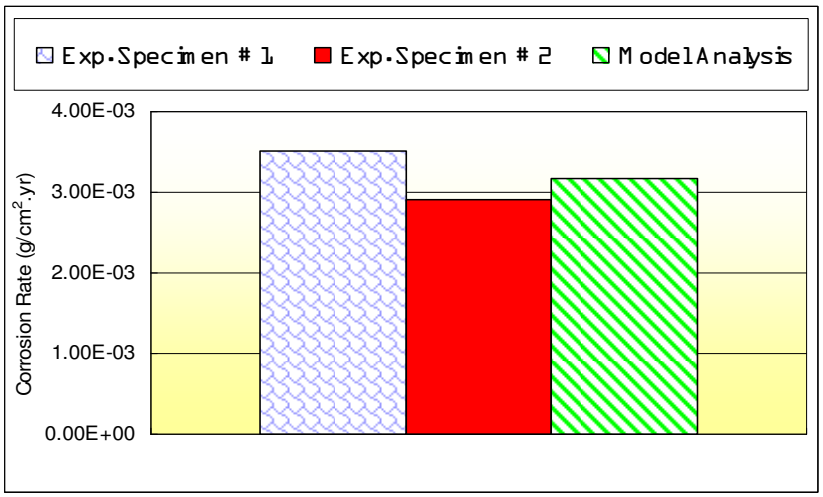

Figure 8. Verification of carbonation induced corrosion model

8. CONCLUSIONS AND SCOPE FOR FUTURE RESEARCH

The half-cell potential values of corroding rebars fluctuate with the time and depth of carbonation. The half-cell potential of rebar in non-carbonated and fully carbonated concretes varies between -180mV CSE and -475mV CSE. The carbonation induced corrosion cannot start until the carbonation depth reaches a certain critical level of depth from the steel rebar. This critical carbonation depth has been calculated as 80% of the total depth of concrete cover in this research. As the carbonation reaction

proceeds, the resistivity of concrete increases which reduces the electrolytic conductivity of the pore solution resulting in reduction of the corrosion rate. Therefore, it can be said that the carbonation induced corrosion has a falling trend with the passage of time. The corrosion rate due to carbonation under air dry humidity condition (55%-60% R.H) is calculated as 0.325μA/cm^2 which is much lower than chloride induced corrosion rate. The carbonation induced corrosion model reasonably predicts the behaviour of corrosion for normal air dry relative humidity conditions at carbonation level of pH 8.0. The model also shows fair qualitative simulation for various pH levels. In the future research quantitative carbonation induced corrosion rate should be investigated experimentally for various relative humidity conditions, different pH levels and combined effects of carbonation and chloride.

References

1. Hamada, M., Concrete carbonation and steel corrosion, Cement/Concrete, No.272, pp.2-18, 1969.
2. Luca Bertolini, Bernhard Elsener, Pietro Pedeferri, Rob Podler, Corrosion of Steel in Concrete WiLey-VCH GmbH& Co. KGaA, 2000.
3. Vladimir Zivica,"Corrosion of reinforcement induced by environment containing chloride and carbon dioxide" Bull. Material Science., Vol. 26, No. 6, pp. 605–608, October 2003.
4. Nagataki, S., Ohga, H. and Saeki, T.: Analytical prediction of carbonation depth, Annual report of cement technology, No. 41, pp. 343-346. 1987.
5. Saetta, A.V., Schrefler, B.A., and Vitaliani, R.V., The carbonation of concrete and the mechanisms of moisture, heat and carbon dioxide flow through porous materials, Cement and Concrete Research Vol.23, pp.761-772, 1993.
6. Tanano, H. and Masuda, Y.: Mathematical model on progress of carbonation of concrete, Proceedings of JCI, Vol.13, No1, pp.621-622, 1991.
7. Tetsuya Ishida and Koichi Maekawa, Modeling of pH profile in pore water based on mass transport and chemical equilibrium theory, Proceedings of JSCE, No.648/V-47, May 2000 (in Japanese).
8. Ishida, T. and Maekawa, K., An integrated computational system for mass/energy generation, transport, and mechanics of materials and structures, Concrete Library of JSCE, No.36, pp.129-144, 2000.
9. Hussain Raja Rizwan and T. Ishida (2007) Modeling of corrosion in RC structures under variable chloride environment based on thermodynamic electro-chemical approach, Journal of SSMS, JAPAN. SMS07-106/2007, Vol.3, p.p:104-113. (Best paper award for the last four years 2005-2009. online: http://management.kochi-tech.ac.jp/society_approve.php).
10. Koichi Maekawa, Tetsuya Ishida and Toshiharu Kishi, Multi-scale Modeling of concrete performance. Joural of Advanced Concrete Technology, Vol. 1, No. 2, pp.91-126,2003 .
11. Welty, J.R., Wicks, C.E., and Wilson, R.E.: Fundamentals of momentum, heat, and mass transfer, John Wiley& Sons, Inc., 1969.
12. Saeki, T., Ohga, H. and Nagataki, S., Mechanism of Carbonation and Prediction of Carbonation Process of Concrete, Concrete Library of JSCE, No.17, pp.23-36, 1991.
13. Papadakis, V.G., Vayenas, C.G. and Fardis, M.N.: Fundamental modeling and experimental investigation of concrete carbonation, ACI Material Journal, pp.363-373, Vol.88, No.4, 1991.
14. Maekawa, K., Kishi, T. and Chaube, R. P.: Modelling of Concrete Performance, E&FN SPON,1999.
15. Kunii, T. and Hurusaki, S.: The Theory on Transfer Rate, Bai-hu Kan press, 1980.
16. Kobayashi, K., Syutto, K.: Diffusivity of oxygen in cementitious materials, Concrete Engineering, Vol.24, No.12, pp.91-106, 1986.
17. Cusack, N. E., The Physics of Structurally Disordered Matter, Bristol edition, 1987.

18. Fritz Haber and Zygmunt Klemensiewicz, Uber electrischie Phasengrenzrafte Z. phys. Chem., 67., 385, 1909.
19. Jui H. Wang and Eva Copeland "Equilibrium Potentials of Membrance Electrodes" Proceedings of the national academy of sciences of the United States of America Vol. 70, No. 7 pp. 1909-1911,(Jul., 1973).
20. ASTM C 876-91, "Standard test method for half-cell potentials of uncoated reinforcing steel in concrete", ASTM, U.S.A, 1999.
21. ASTM G1-03, "Standard test practice for evaluating corrosion test", ASTM, U.S.A, 2002.
22. Luca Bertolini, Bernhard Elsener, Pietro Pedeferri, Rob Podler, Corrosion of Steel in Concrete WiLey-VCH GmbH& Co. KGaA, 2000.